Anti-reflection high-index metasurfaces combining Mie and Fabry–Pérot resonances

Andrea Cordaro,[†,‡,¶] Jorik van de Groep,[†] Søren Raza,[†,§] Emanuele Francesco Pecora,[†] Francesco Priolo,[‡,¶] and Mark L. Brongersma[*,†]

†*Geballe Laboratory for Advanced Materials, Stanford University, Stanford, California 94305, United States*

‡*Dipartimento di Fisica e Astronomia "Ettore Majorana", Università di Catania, via S. Sofia, 64, 95123 Catania, Italy*

¶*Scuola Superiore di Catania, Università di Catania, via Valdisavoia, 9, 95123 Catania, Italy*

§*Department of Physics, Technical University of Denmark, DK-2800 Kongens Lyngby, Denmark*

E-mail: brongersma@stanford.edu

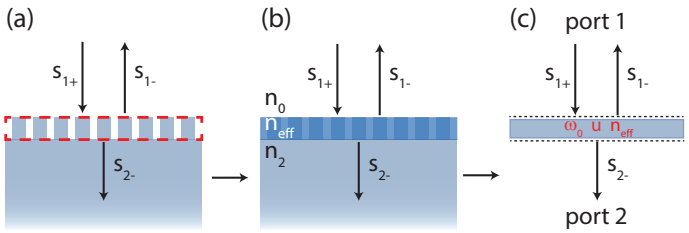

Figure 1: Schematic of a two-ports coupled resonator: (a) the resonators are enclosed into a “box” (dashed red) that define the optical system (b) the direct pathway is given by the scattering matrix of a dielectric film of an effective index between two semi-infinite optical media (c) final scheme for CMT; the dashed lines indicate the input/output planes.

Coupled Mode Theory

Coupled Mode Theory (CMT) is the closest mathematical translation to the intuitive explanation of the working principle of the structure given in the main text.

The first step of theoretical derivation consists in defining the optical system and the output and input planes. Hence, suppose the resonant structures (nanopillars or nanowires arrays) are enclosed inside a “black box" (see Fig. (1)a) simply stating that the complex field inside the box is u (normalized such that $|u|^2$ is the energy stored within the box due to the resonance) and that this system has a certain resonance frequency ω_0.

Furthermore, the system is coupled to two input/output ports being $\mathbf{s}_+$ and $\mathbf{s}_-$ the column vectors containing, respectively, the incoming and outgoing wave amplitudes from each channel (or port). The complex wave amplitudes are defined and normalized such that, for example, $|s_{1+}|^2$ is the power per unit area incident on the the system (see Fig. (1)) $s_{1+} = \sqrt{\frac{cn_0\epsilon_0}{2}}\mathbf{E}_{1+}$, with analogous definitions for the remainder components of the vectors $\mathbf{s}_-$ and $\mathbf{s}_+$.[1]

Within the CMT formalism, the outgoing wave amplitudes $\mathbf{s}_-$ are the result both of the box’s leakage and of the action of a scattering matrix C, which would describe the system if the resonances were turned off, to the incoming wave amplitudes $\mathbf{s}_+$

$$\mathbf{s}_- = \mathsf{C}\,\mathbf{s}_+ + u\,\mathbf{d} \tag{1}$$

where $\mathbf{d} = (d_1, d_2)^\top$ is a vector of coupling coefficients. Starting with the lossless case, the direct

process is modeled by the interaction of light with a dielectric slab of index n_{eff} (see Fig. (1)b) between two semi-infinite media with indices n_0 and n_2 ($\in \mathbb{R}$). Thus in our model Eq.1 is

$$\begin{pmatrix} s_{1-} \\ s_{2-} \end{pmatrix} = \begin{pmatrix} r_{12} & t\sqrt{\frac{n_2}{n_0}} \\ t\sqrt{\frac{n_2}{n_0}} & r_{21} \end{pmatrix} \begin{pmatrix} s_{1+} \\ 0 \end{pmatrix} + u \begin{pmatrix} d_1 \\ d_2 \end{pmatrix} \tag{2}$$

where r_{12} and t are the standard Fresnel coefficients for a field propagating towards the substrate and r_{21} is the Fresnel reflection coefficient for a field propagating from the substrate.

Equation (2) shows clearly that the output of the optical system is the sum of a direct process (first product in the right-hand side) and a resonant process (second product in the right-hand side). Notice that s_{2+} is zero since no light is coming from the substrate and that writing the scattering matrix in the above form fixes the reference planes (see Fig. (1)) to be the interfaces between the three media (n_0 / n_{eff} / n_2).

Coupled to (2), another equation is needed to describe the complex field inside the system

$$\frac{du}{dt} = (i\omega_0 - \gamma_1 - \gamma_2)\, u + \kappa_1 s_{1+} \tag{3}$$

being γ_1 the leakage rate upwards, γ_2 the leakage rate into the substrate and κ_1 the coupling coefficient for s_{1+} pumping the resonator[1]. If the incoming wave amplitude has an harmonic time dependence also u will and $\frac{d}{dt} \to i\omega\cdot$, therefore from (3) and (2) it is easy to retrieve the quantity

$$\Gamma = \frac{s_{1-}}{s_{1+}} = r_{12} + \frac{d_1\kappa_1}{i(\omega - \omega_0) + \gamma_1 + \gamma_2} \tag{4}$$

This last quantity is of great importance in our derivation since the reflectance of the whole system is $R = |\Gamma|^2$ as can be noted recalling the definitions of $\mathbf{s}_-$ and $\mathbf{s}_+$. Since the reflection itself is bound to be $R \leqslant 1$ it is quite intuitive that the coupling coefficients showing in the last equation cannot take arbitrary values. Indeed, these are constrained by the non-resonant pathway through properties that are a direct consequence of fundamental concepts such as energy conservation and

[1] κ_1 is the first component of the vector $\boldsymbol{\kappa}$ of coupling coefficients

time-reversal symmetry[2–4]

$$\mathbf{d}^{\dagger}\mathbf{d} = 2\gamma \tag{5}$$

$$\boldsymbol{\kappa} = \mathbf{d} \tag{6}$$

$$\mathsf{C}\,\mathbf{d}^{*} = -\mathbf{d} \tag{7}$$

where C is a generic scattering matrix describing the direct pathway and γ is the sum of the leakage rates into the ports. Using the latter properties and those applying to scattering matrices for lossless media (i.e. $\mathsf{C}^{\dagger}\mathsf{C} = \mathbb{I}$) it is possible to further refine the expression obtained for Γ and to deduce an expression for d_1^2

$$\Gamma = r_{12} + \frac{d_1^2}{i(\omega - \omega_0) + \gamma_1 + \gamma_2} \tag{8}$$

$$d_1^2 = \frac{-(2\gamma_1)^2 e^{i\theta_{12}}}{\frac{1}{|r|}(\gamma_1 - \gamma_2) + |r|(\gamma_1 + \gamma_2) \pm \sqrt{\frac{1}{|r|^2}(\gamma_1 - \gamma_2)^2 + |r|^2(\gamma_1 + \gamma_2)^2 - 2(\gamma_1^2 + \gamma_2^2)}} \tag{9}$$

where $r_{12} = |r|e^{i\theta_{12}}$ was set. This last result is very similar to and in agreement with that of Wang et al.[4] The quantity Γ is the sum of two terms: r_{12} is the Fresnel coefficient for a dielectric slab on a substrate and plays the role of the *direct pathway* mentioned earlier while the second term is due to the resonant behavior displayed by the structure and hence is referred to as *resonant pathway*. Furthermore, the resonant path itself contains the direct path (Eq.9) as a consequence of the constraints shown earlier.

So far, only the lossless case has been taken into account. Nonetheless, given that the metasurfaces are etched directly into silicon, internal absorption cannot be ignored. Following the example of Ruan et al.,[5] internal loss is included only within the resonant pathway thus keeping the scattering matrix unitary. Of course, this is already an approximation to our original model. The addition of an extra loss rate γ_0 due to absorption in (3) would result in a new expression for Γ

$$\Gamma = r_{12} + \frac{d_1^2}{i(\omega - \omega_0) + \gamma_0 + \gamma_1 + \gamma_2} \tag{10}$$

Approximation

The main purpose of the theoretical derivation is to find a relatively easy expression for the reflectance that can reproduce the spectra obtained by FDTD simulations. One might be tempted to use (10) however this is not possible due to the presence of diffraction within the substrate that confines its validity to the portion of Figure 2 in which $\lambda > n_2\, p$. Indeed, the arrays are surely sub-wavelength for visible light on the air side but the same does not hold for the substrate, especially if it is a high index dielectric as silicon. In other words the structure acts as an effective layer in reflection but as a grating in transmission as soon as $\lambda \leqslant n_2\, p$.

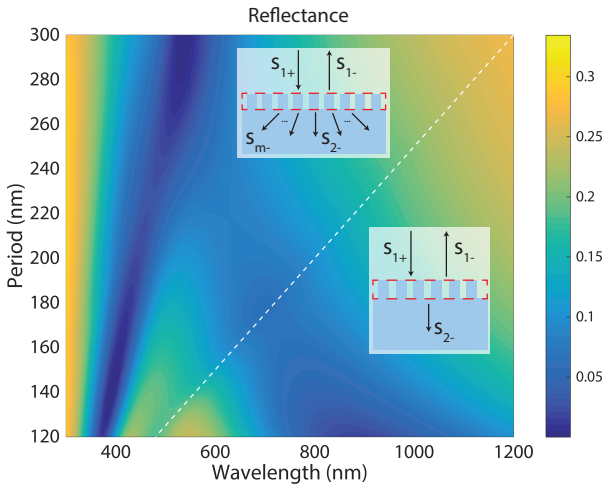

Figure 2: FDTD-simulated reflectance of an array of nanowires (individual wire $120\,nm \times 80\,nm$) as p and λ change. The white dashed line remarks the onset of diffraction. Insets: schematics of *two–ports* and *m-ports* coupled resonators.

Taking diffraction into account in the CMT formalism means adding a new port for every diffraction channel opened, which in turn means changing the dimension of the scattering matrix accordingly and adding the appropriate number of leakage rates. This is the reason why (10) cannot be used to fit the simulated reflectance colormap. First, the expression is so complicated due to the presence of d_1 that the fitting algorithm rarely converges. Further, since diffraction was not included in our derivation, even if the fit converged it would to wrong values of the leakage rates. Updating the model to an *m-port* configuration would not accomplish our goal of obtaining

a simple model grasping the physical meaning of the spectra.

In search of a feasible approximation, it is useful to quickly go through the main points of the previous derivation trying to grasp the differences as the formalism is extended to *m-ports* (see Fig. (2) for the new scheme). The *m-ports* versions of (2) and (3) are respectively

$$\begin{pmatrix} s_{1-} \\ s_{2-} \\ \vdots \\ s_{m-} \end{pmatrix} = \begin{pmatrix} C_{11} & C_{12} & \cdots & C_{1m} \\ C_{21} & C_{22} & \cdots & C_{2m} \\ \vdots & \vdots & \ddots & \vdots \\ C_{m1} & C_{m2} & \cdots & C_{mm} \end{pmatrix} \begin{pmatrix} s_{1+} \\ 0 \\ \vdots \\ 0 \end{pmatrix} + u \begin{pmatrix} d_1 \\ d_2 \\ \vdots \\ d_m \end{pmatrix} \tag{11}$$

$$\frac{du}{dt} = \left(i\omega_0 - \sum_i \gamma_i \right) u + d_1 s_{1+} \tag{12}$$

It is crucial to notice that even if extra channels in transmission are opened there is always one single channel in reflection. As a consequence, Γ is still defined as s_{1-}/s_{1+} and its absolute square will still give the reflectance of the system. Following in our own footsteps

$$\Gamma = \frac{s_{1-}}{s_{1+}} = C_{11} + \frac{d_1^2}{i(\omega - \omega_0) + \sum_i \gamma_i} \tag{13}$$

At this point two main routes opens up ahead: either one tries to give an expression to every matrix element and then embarks himself on solving $\mathsf{C}\mathbf{d}^* = -\mathbf{d}$ to find the new d_1 or tries to approximate the resonant and direct pathways showing in this last equation. Here the second choice has been preferred.

Starting from the resonant pathway, it is conceivable to say that it is basically a Lorentzian whose amplitude, width and phase are related to the direct path and to the leakage rates in a rather complicated manner. Regarding the direct path, it can be argued that light is still seeing an effective layer (there is no diffraction in air) but once diffraction channels are opened energy is redistributed to more ports resulting in a little decrease in reflection and in anomalies in the spectrum known as *Rayleigh's anomalies*. In any case, since the knowledge of C_{11} is related to that of all the other elements (recall the $\mathsf{S} - matrix$ properties), here it is simply assumed that r_{12} is still a feasible

approximation even when diffraction is present. With these assumptions and a minor change in notation ($r_{12} \rightarrow r_{eff}$), the expression used in the main text for the reflectance is

$$R = \left| r_{12} + \frac{A \ e^{i\phi}}{i(\omega - \omega_0) + g} \right|^2 \tag{14}$$

Design

The following section explains the design routine adopted to obtain the optimized geometries for the Si[6] nanowires and nanopillars arrays presented in the main text. The first step of such optimization consists in exploring how the Mie resonances of a single scatterer are influenced by the geometry.

Figure (3)a shows the normalized scattering cross section (scattering cross section normalized to the geometrical cross section) Q_{scatt} for a rectangular nanowire ($w \times 3/2\, w$) as the width w and the wavelength are changed if incoming light is at normal incidence and with a polarization such that $\mathbf{E}$ is perpendicular to the wires. It is easy to notice that the first available mode lies in the visible spectrum if $w \lesssim 120\, nm$ while higher order modes are excited at shorter wavelengths. Since, inter-wire coupling is expected to blue-shift the resonance wavelength, the width chosen is $w = 80\, nm$ which has a resonance around $\lambda \simeq 570\, nm$.

The choice of a rectangular nanowire ($3 : 2$) may seem quite random. Indeed, for the nanowire's fundamental mode the height is relevant only to some extent. To prove this, Q_{scatt} for a single wire of fixed width $w = 80\, nm$ has been calculated as its height is swept from $60\, nm$ to $200\, nm$ (see Fig. (3)b). The change in height induces only a small shift of the resonance frequency which saturates above $h \simeq 170\, nm$, in agreement with the result of Van de Groep et al.[7] Inspection of the fields profiles allows labeling the mode as a Magnetic Dipole (MD) resonance (see Fig. (3)c). The low sensitivity of the MD mode to the wire height enables us to tune h at will.

On the other hand, the nanowires' height defines the thickness of the effective layer and therefore influences the direct pathway. To have a physical intuition of this phenomenon, a reflectance

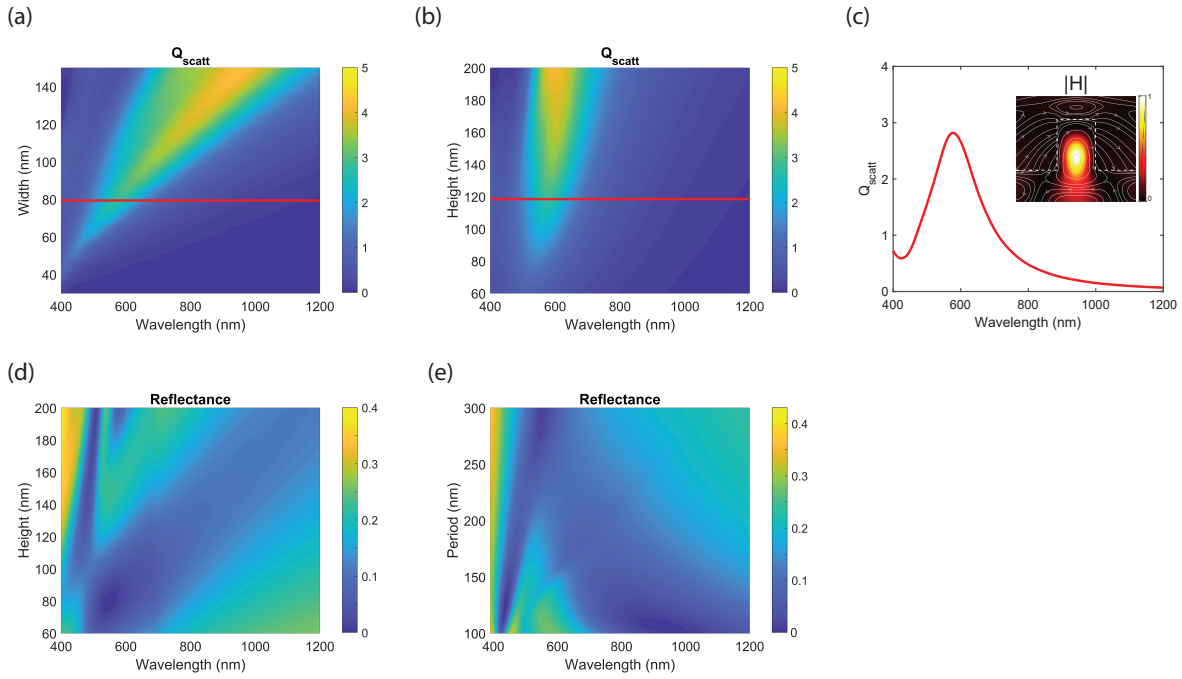

Figure 3: (a) Q_{scatt} for a rectangular Si nanowire $(3:2)$ as the width w and the wavelength are changed. (b) Q_{scatt} for a rectangular Si nanowire of fixed width $w = 80\,nm$ as the height h and the wavelength are changed. (c) Q_{scatt} for a rectangular Si nanowire of fixed width $w = 80\,nm$ and height $h = 120\,nm$. Inset: magnetic field amplitude profile and $\mathbf{E}$ field lines at the peak wavelength of Q_{scatt}. (d) Reflectance colormap for an array of Si nanowires with fixed width $w = 80\,nm$ and fixed periodicity $p = 180\,nm$ as the height of the wires is changed. (e) Simulated reflectance of an array of Si nanowires (individual wire $80\,nm \times 120\,nm$) as p and λ change. The substrate is Si for all of the panels.

colormap is calculated for an array of nanowires with fixed width $w = 80\,nm$ and fixed periodicity $p = 180\,nm$ (thus fixed n_{eff}) as the height of the wires is changed (see Fig. (3)d). Both reflection minima are shifting to longer wavelength as h increases but the minimum due to the Fabry–Pérot resonance shows much higher sensitivity to h. The dashed white line of Figure 1c of the main text is shifting to lower frequencies and this is in agreement with the fact that a thicker layer can fit longer wavelengths. Finally, the thickness chosen is $120\,nm$ which corresponds to a dip around $\lambda \simeq 700\,nm$ for this periodicity.

It is important to point out that changing either the height or the width affects both the pathways although, as just shown, to some extent it is possible to choose h and w separately. Figure (3)e depicts the reflectance colormap of a Si nanowires array $80\,nm \times 120\,nm$ which is the final re-

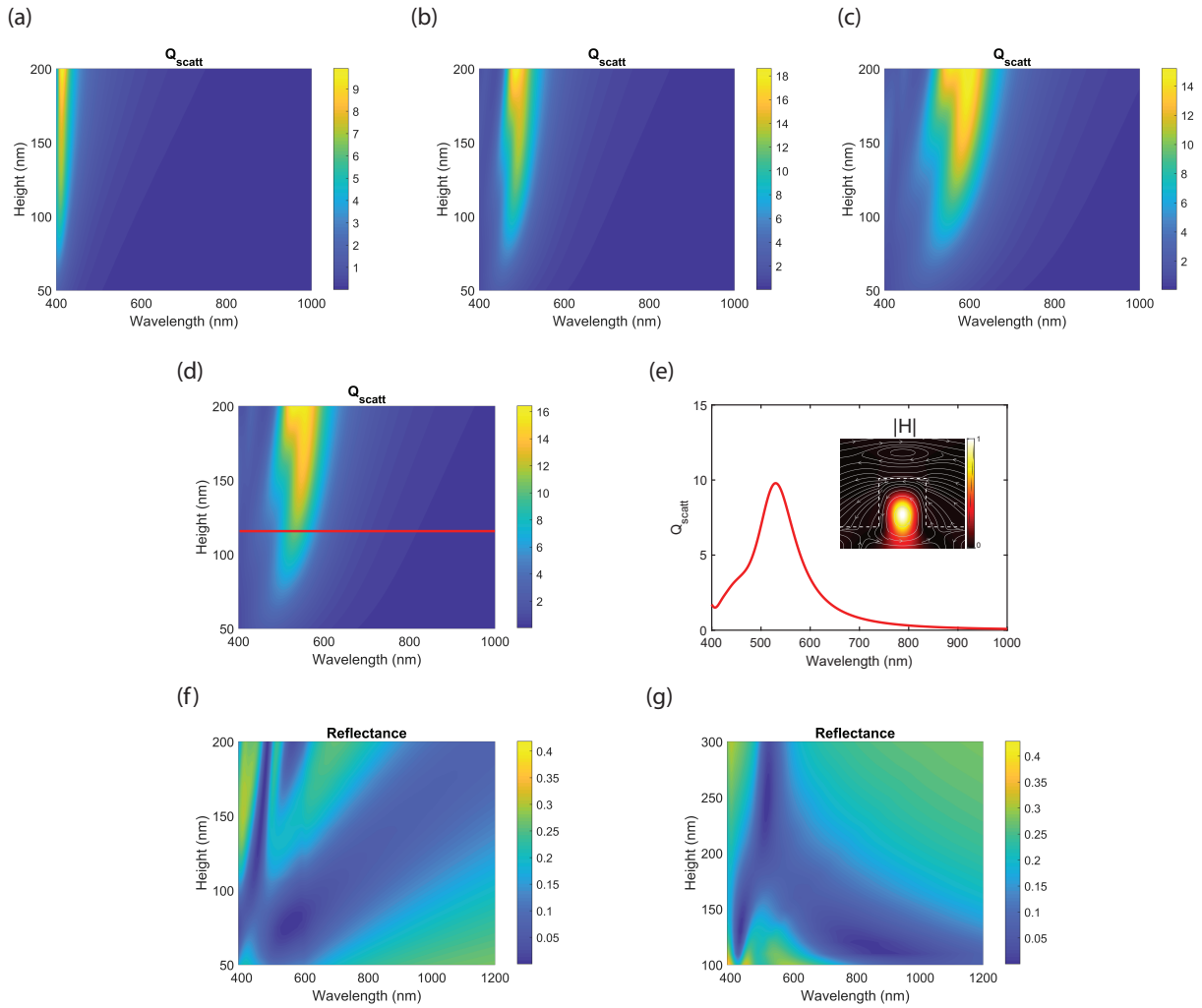

Figure 4: (a-c) Q_{scatt} for a square–based Si nanopillar of fixed width $w = 50\,nm$, $w = 75\,nm$ and $w = 100\,nm$ as the height h and the wavelength are changed. (d) Q_{scatt} for a square–based Si nanopillar of fixed width $w = 90\,nm$ as the height h and the wavelength are changed. (e) Q_{scatt} for a square–based Si nanopillar of fixed width $w = 90\,nm$ and height $h = 110\,nm$. Inset: magnetic field amplitude profile and $\mathbf{E}$ field lines at the peak wavelength of Q_{scatt}. (f) Simulated reflectance for an array of square–based Si nanopillar with fixed width $w = 90\,nm$ and fixed periodicity $p = 150\,nm$ as the height of the wires is changed. (g) Simulated reflectance for an array of square–based Si nanopillar (individual pillar $90\,nm \times 90\,nm \times 110\,nm$) as p and λ change. The substrate is Si for all of the panels.

sult of this design procedure. A similar analysis can be performed for the case of square–based nanopillars yielding similar results. In the latter case, however, also the Electric Dipole (ED) mode is present as a shoulder of the dominant MD mode.[7] This is confirmed by the field profile shown in the inset of Fig. (4)e, which shows again the characteristic Magnetic Dipole profile. Analogously to the nanowire case, the width $w = 90\,nm$ is chosen as it exhibits a MD resonance around $\lambda \simeq 530\,nm$ (see Figs. (4)d-e). Finally the height of the pillars is chosen as ($h = 110\,nm$) such that the Fabry–Pérot minimum is around $\lambda \simeq 710\,nm$ (see Fig. (4)f). Figure (4)g shows the reflectance colormap of a square–based Si nanopillar array $90\,nm \times 90\,nm \times 110\,nm$ as the periodicity p is swept from $100\,nm$ to $300\,nm$.

Slanting

The consequences of slanted sidewalls on the resonant and on the direct path are isolated and analyzed. Concerning the direct pathway, the following approximation has been done to include the effects of slanting. The nanowires in Figure (5)a were approximated by a set of slabs of different width but same height resembling Mayan pyramids. Each level of the pyramids has a specific filling fraction (the periodicity is kept fixed at $p = 180\,nm$) and therefore is seen by incident light as an effective layer with a certain effective index given by Eq.(1) of the main text. Thus the direct pathway of slanted nanowires is approximated by n effective layers and changing the angle of the sidewalls is accounted for by changing the set of effective indices (Figure (5)a). As can be easily noticed by inspection of Figure (5)b the consequences of slanting are a blue-shift of the first Fabry–Pérot minimum and a general reduction in reflection. The reason behind this beneficial effect is that the abrupt discontinuity in the index is partially removed and, to some extend, a graded index AR coating in only $120\,nm$ is generating the direct pathway.

On the other hand, to study how the resonant pathway is affected, the scattering cross section σ_s of a single wire is monitored. Changing the sidewalls slanting as described previously, the consequent variation in σ_s is shown in the colormap in Figure (6)a. Peculiarly, the resonance

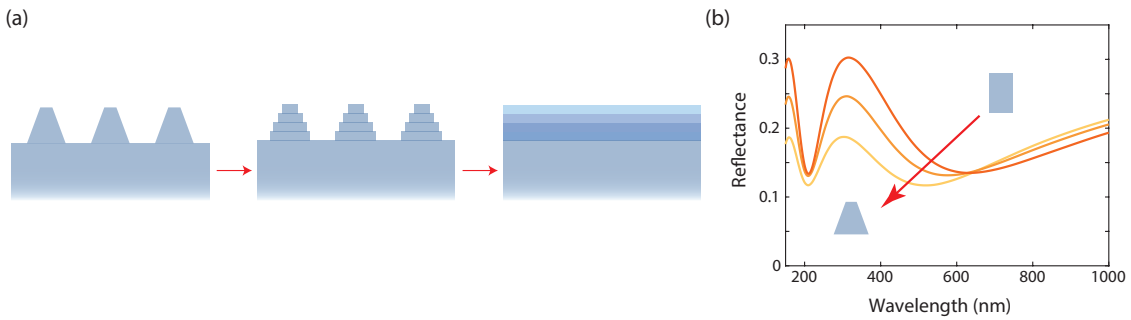

Figure 5: (a) Slated nanowires–to–effective layers approximation for the direct pathway. (b) Simulated reflectance of 4 layers on a Si (non-dispersive model used in the main text) substrate as their effective indices are changed according to the approximation.

broadens and red-shifts. To understand why this is happening also the fields profiles should be inspected (see Figure (6)b-d). Clearly, the characteristic displacement current loops of the MD

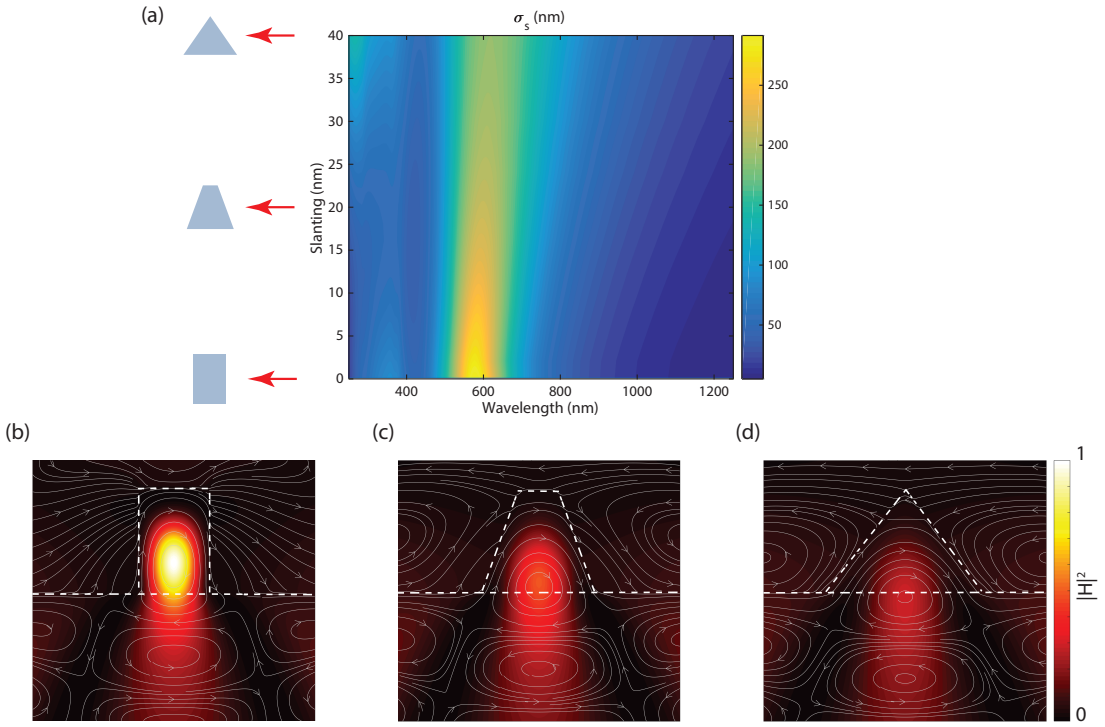

Figure 6: (a) Scattering cross section for a Si nanowire as λ and the sidewalls slanting are changed. (b-d) Fields profiles ($\mathbf{E}$ field lines in gray and $\mathbf{H}$ filed intensity as a colormap) for the magnetic dipole resonance as the sidewalls slanting is changed.

mode are moving closer to the substrate as the sidewalls become tilted, this in turn means that the resonator is more coupled to the substrate and the leakage rate into it increases implying a

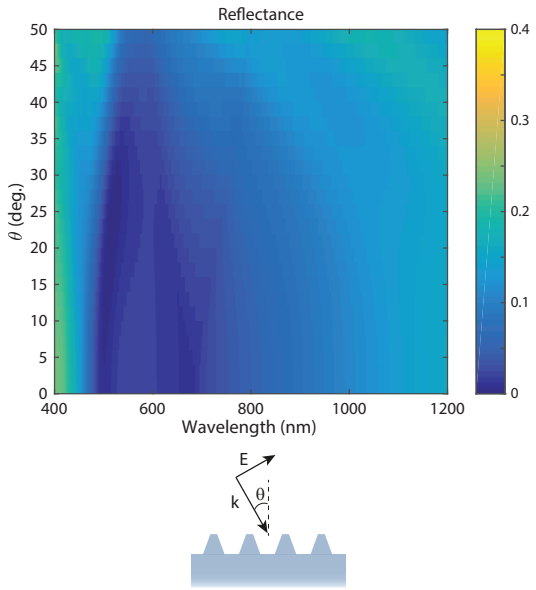

Figure 7: Simulated angle–resolved reflectance for an array of slanted Si nanowires on a Si substrate. The shape, sizes and periodicity of the wires are the same of those used in Fig.3 of the main text.

broadening of the resonance. The same conclusion can be drawn by looking at the **H** field intensity colormap. In addition, the lateral dimension of the current loops increases with slanted sidewalls thus the "effective resonator" is wider and its resonance frequency red-shifts. At this point all the ingredients to give an intuitive interpretation of why the double dip merges into a broad single dip are available. Indeed, the resonant pathway is broadening and red-shifting while the direct pathway is blue-shifting and generally decreasing. Thus, intuitively the red and white dashed lines of Figure 1c of the main text are getting closer as the tilting of the sidewalls is increasing. In addition, the average reflection is lower because both the scattering and the contribution from the direct pathway are less intense.

Angle–resolved Reflectance

For practical applications, a good anti-reflection response is desirable also for angles of incidence different from normal incidence. Figure (7) shows the simulated reflection spectra, as a function of the incident angle θ, for an array of slanted nanowires with shape, lateral size and periodicity

as in Fig.3 of the main text. Interestingly, the broad double–dip behavior is present and arguably effective up to high angles. In fact, the Mie resonance is still excited giving rise to a reflection minimum in the blue side of the spectrum while, at longer wavelengths, the metasurface response is analogous to that of a slab of index n_{eff} (given by Eq.1 of the main text) on Si substrate (see Fig. (8)a-b). The latter point is further stressed in Fig. (8)c.

In conclusion, the concept of combining Mie and Fabry–Pérot resonances for effective anti-reflection holds also for $\theta \neq 0$ and can be used for further optimization for practical applications.

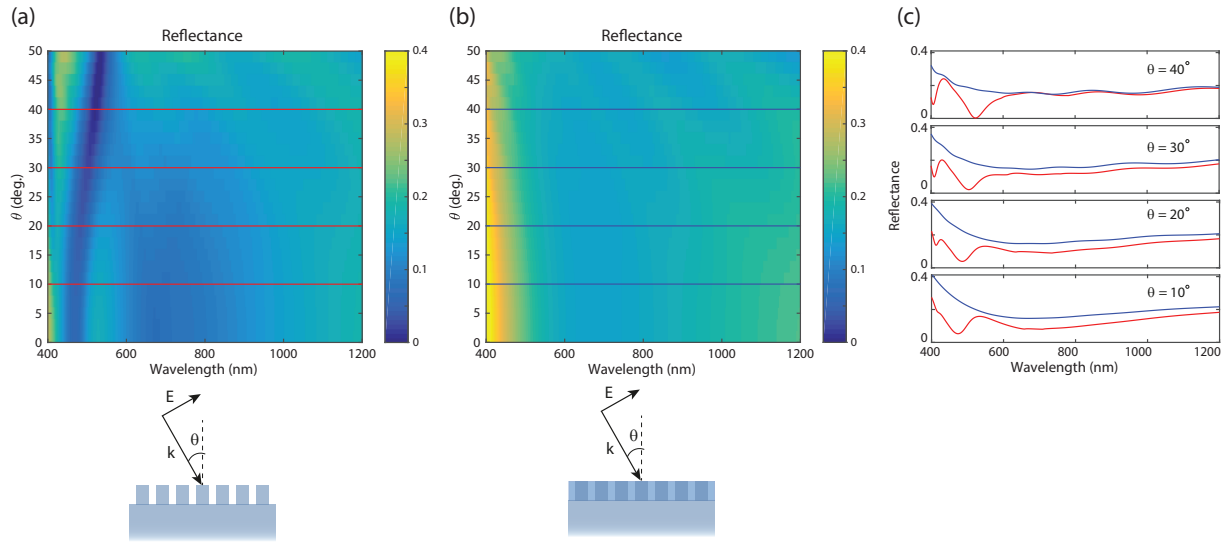

Figure 8: (a) Simulated angle–resolved reflectance for an array of Si nanowires on a Si substrate($p = 180nm$, $w = 80nm$ and $h = 120nm$). (b) Simulated angle–resolved reflectance for a slab of index n_{eff} (given by Eq.1 of the main text) and thickness $h = 120nm$ on a Si substrate. (c) Line–cuts through (a) (red) and (b) (blue).

Optical microscopy images

Figure (9) shows optical microscopy images of the samples described in the main text. For the case of the nanowires, we emphasize the strong difference in reflection for the perpendicular and parallel polarization respectively. On the contrary, the nanopillar arrays show no dependence on incoming light polarization.

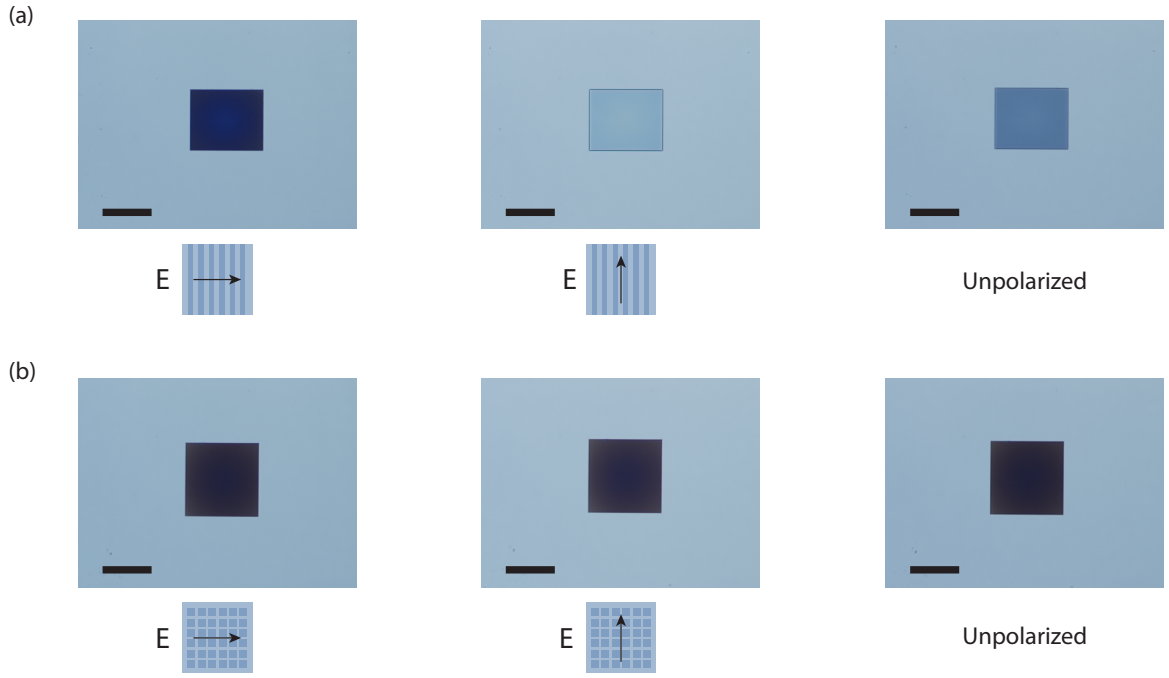

Figure 9: Optical microscopy images of the nanowire array (a) and nanopillar array (b) samples illuminated with different polarization as well as unpolarized light. The scale-bar is $50\mu m$

References

(1) Haus, H. *Waves and fields in optoelectronics*; Prentice-Hall Series in Solid State Physical Electronics; Prentice Hall, Incorporated, 1984.

(2) Fan, S.; Suh, W.; Joannopoulos, J. D. Temporal coupled-mode theory for the Fano resonance in optical resonators. *J. Opt. Soc. Am. A* **2003**, *20*, 569 – 572.

(3) Wang, K. X.; Yu, Z.; Sandhu, S.; Fan, S. Fundamental bounds on decay rates in asymmetric single-mode optical resonators. *Opt. Lett.* **2013**, *38*, 100–102.

(4) Wang, K. X.; Yu, Z.; Sandhu, S.; Liu, V.; Fan, S. Condition for perfect antireflection by optical resonance at material interface. *Optica* **2014**, *1*, 388–395.

(5) Ruan, Z.; Fan, S. Temporal Coupled-Mode Theory for Fano Resonance in Light Scattering by a Single Obstacle. *The Journal of Physical Chemistry C* **2010**, *114*, 7324–7329.

(6) Palik, E. *Handbook of Optical Constants of Solids*; Academic Press handbook series 3; Academic Press, 1998.

(7) van de Groep, J.; Polman, A. Designing dielectric resonators on substrates: Combining magnetic and electric resonances. *Opt. Express* **2013**, *21*, 26285–26302.